Photoinduced Ultrafast Intramolecular Excited-State Energy Transfer in the Silylene-Bridged Biphenyl and Stilbene (SBS) System: A Nonadiabatic Dynamics Point of View

ARTICLE *in* THE JOURNAL OF PHYSICAL CHEMISTRY A · MAY 2015

Impact Factor: 2.69 · DOI: 10.1021/acs.jpca.5b00354 · Source: PubMed

THE JOURNAL OF PHYSICAL CHEMISTRY A

Article

pubs.acs.org/JPCA

Photoinduced Ultrafast Intramolecular Excited-State Energy Transfer in the Silylene-Bridged Biphenyl and Stilbene (SBS) System: A Nonadiabatic Dynamics Point of View

Jun Wang,[†,‡] Jing Huang,[†,‡] Likai Du,[†,‡] and Zhenggang Lan*[,†,‡]

[†]Key Laboratory of Bio-based Materials, Qingdao Institute of Bioenergy and Bioprocess Technology, Chinese Academy of Sciences, Qingdao, 266101 Shandong, P. R. China

[‡]University of Chinese Academy of Sciences, Beijing 100049, P. R. China

Supporting Information

ABSTRACT: The photoinduced intramolecular excited-state energy-transfer (EET) process in conjugated polymers has received a great deal of research interest because of its important role in the light harvesting and energy transport of organic photovoltaic materials in photoelectric devices. In this work, the silylene-bridged biphenyl and stilbene (SBS) system was chosen as a simplified model system to obtain physical insight into the photoinduced intramolecular energy transfer between the different building units of the SBS copolymer. In the SBS system, the vinylbiphenyl and vinylstilbene moieties serve as the donor (D) unit and the acceptor (A) unit, respectively. The ultrafast excited-state dynamics of the SBS system was investigated from the point of view of nonadiabatic dynamics with the surface-hopping method at the TDDFT level. The first two excited states (S_1 and S_2) are characterized by local excitations at the acceptor (vinylstilbene) and donor (vinylbiphenyl) units, respectively. Ultrafast S_2—S_1 decay is responsible for the intramolecular D—A excitonic energy transfer. The geometric distortion of the D moiety play an essential role in this EET process, whereas the A moiety remains unchanged during the nonadiabatic dynamics simulation. The present work provides a direct dynamical approach to understand the ultrafast intramolecular energy-transfer dynamics in SBS copolymers and other similar organic photovoltaic copolymers.

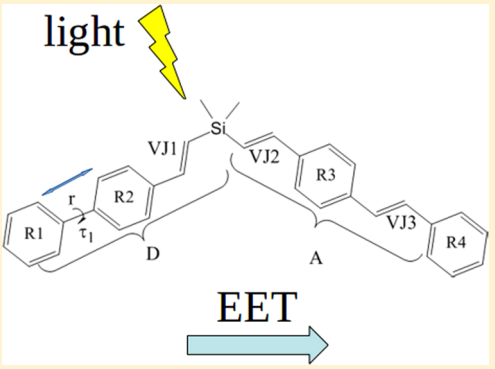

1. INTRODUCTION

Linear polymers composed of many different π-conjugated units connected by silylene bridges have received considerable research interest in recent years because of their potential applications in photovoltaic and photoelectric materials.[1−5] Because the silylene moieties effectively interrupt π-conjugation along the polymer chain,[3] the whole system can be treated as an ensemble of several interacting individual conjugated units. Thus, their photophysical and photochemical properties can easily be controlled through the modification of each π-conjugated chromophore.[6]

In principle, photoinduced interchain and intrachain excited-state energy-transfer (EET) processes should be widespread in organic conjugated copolymers.[3,6−17] As this is an essential photophysical process, intramolecular EET among different conjugated units in Si-linked oligothiophenes or polymers has been widely studied in recent years.[1,11,18−20] In a series of joint experimental/theoretical works by Liu et al., a few silylene-spaced copolymers consisting of electron-donor (D) units (biphenyl), electron-acceptor (A) units (stilbene), and silylene bridges, including $(DA)_m$ and $(D_3A)_m$, were studied.[19,20] In time-resolved experiments, these two copolymers were found to show similar ultrafast (∼300 fs) intramolecular D—A EET processes. The similarity of the EET time scales strongly implies that the ultrafast energy transfer involves only two adjacent D and A units. In their theoretical studies,[19,20] the same group employed the standard Förster model[21] and the Fermi golden rule[10,22] to understand the D—A EET mechanism.[8,20] With these theoretical models, the computed D—A EET rates were consistent with the experimental observations.[20]

Although the above studies provided useful information for understanding the intramolecular EET process of silylene-bridged biphenyl and stilbene (SBS) copolymers, it is very difficult to elucidate all of the details of such EET processes. For example, what are the real-time excited-state molecular motions, and which internal nuclear coordinates are involved? Such details can be addressed by exciton motion based on the theory of the electronic density matrix.[23,24] Although it is not a trivial task to include the correct description of the electron−nuclear coupling terms, particularly the vibronic couplings on molecular excited states, in such a theoretical framework, the

Received: January 13, 2015
Revised: May 13, 2015
Published: May 27, 2015

DOI: 10.1021/acs.jpca.5b00354
J. Phys. Chem. A 2015, 119, 6937−6948

effects of realistic electron−nuclear couplings should not be neglected because of the ultrafast time scale of the EET process. Thus, to provide a more direct understanding of the EET process in SBS copolymers, nonadiabatic dynamics simulations are necessary.

In recent years, the on-the-fly surface-hopping method has become a powerful and practical tool for simulating general photoinduced processes of polyatomic molecular systems at an all-atom level.[25−30] With this tool, interesting results have been derived to understand the photoinduced reactions of organic photovoltaic systems, particularly their excited-state charge-transfer and energy-transfer processes.[28,31−34]

In this work, we employed the on-the-fly trajectory surface-hopping (TSH) method at the time-dependent density functional theory (TDDFT) level to study the intramolecular EET process of a model system: the silylene-bridged biphenyl and stilbene (SBS) system. This system serves as a prototypical system for identifying similar EET processes between the donor and acceptor units of SBS copolymers. The performances of different functionals were carefully examined. The photoactive nuclear motions responsible for the ultrafast EET process were identified. To investigate the EET process more directly, we monitored the evolution with time of two local-excitation (LE) components (i.e., D → D and A → A) that were constructed from the single-electron transition density matrix. We believe that this work should provide an interesting view to understand the EET process of the SBS system, as well as similar photoinduced processes of SBS copolymers and other organic silylene-bridged copolymers.

2. THEORETICAL MODEL AND COMPUTATIONAL DETAILS

2.1. Monomer Structure and Definition of Bond Length Alternation (BLA). The comprehensive investigation of the excited-state dynamics of a polymer at the all-atom level is an impossible task with current computational resources. However, previous works already clarified that the intramolecular EET in silylene-spaced copolymer systems[20] mainly takes place between adjacent biphenyl and stilbene units. Thus, it should be reasonable to focus on the EET process among its building blocks (Scheme 1), which include only a biphenyl unit, a stilbene unit, and a silylene bridge. For convenience, we renamed the building blocks as SBS, and the molecular structure is shown in Scheme 1. As the vinyl junction and the biphenyl unit form an entire conjugated unit, the whole vinylbiphenyl group was taken as the donor (D) unit. On the donor side, the two six-membered rings are labeled as R1 and R2. The single bond connecting these two rings has a length of r, and the associated dihedral angle is given by τ_1. The vinyl junction moiety connecting the biphenyl group is labeled as VJ1. Similarly, we defined the entire vinylstilbene moiety as the acceptor (A) unit. On the acceptor side, the two six-membered rings are labeled as R3 and R4. The vinyl junction moiety connecting the stilbene unit is labeled as VJ2. The vinyl junction moiety between R3 and R4 in the A unit is labeled as VJ3. In addition, the relative orientations of the D and A units can be characterized by the dihedral angles τ_2 and τ_3, respectively.

Scheme 1. Molecular Structures of the SBS System and Its Two Units: the Donor Vinylbiphenyl (D) and the Acceptor Vinylstilbene (A) Moieties[a]

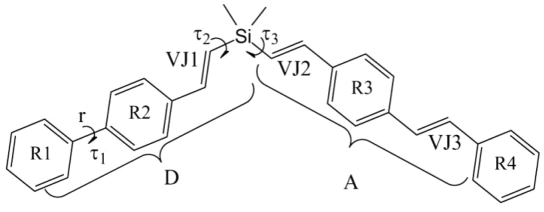

[a]All rings are labeled as R1, R2, R3, and R4. The single bond connecting R1 and R2 has a length of r, and the relevant dihedral angle is given by τ_1. The relative orientations of the D and A units can be characterized by the dihedral angles τ_2 and τ_3, respectively. The vinyl junction moieties are labeled as VJ1, VJ2, and VJ3.

In principle, it is not a trivial task to analyze the in-plane deformations of the six-membered conjugated rings and the vinyl junction moiety because several CC bonds, instead of only a few, can simultaneously experience changes in length. To describe such collective alternation, so-called bond length alternation (BLA, in Scheme 2) coordinates are employed.[35−37]

Scheme 2. Relevant Bond Lengths for the Definition of BLA Parameters: (Left) Phenyl Moiety and (Right) Vinyl Junction

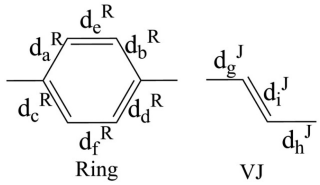

For the six-membered conjugated rings, the BLA parameter d^R is defined as

$$d^R = 0.25(d_a^R + d_b^R + d_c^R + d_d^R) - 0.5(d_e^R + d_f^R) \quad (1)$$

where d_m^R (m = a−f) denotes the length of each CC bond in the ring. Similarly, the BLA parameter d^{VJ} for the vinyl junction moiety is defined as

$$d^{VJ} = 0.5(d_g^{VJ} + d_h^{VJ}) - d_i^{VJ} \quad (2)$$

where d_m^{VJ} (m = g−i) denotes the length of each CC bond in the vinyl junction part.

The BLA parameters, d^R and d^{VJ}, reflect the degrees of conjugation of the conjugated ring and the vinyl junction moiety, respectively, because they provide a direct measurement of the differences in length between the single and double CC bonds that are involved. For example, a smaller value of d^{VJ} indicates the shortening of a single CC bond or the elongation of a double CC bond, implying an increase in the degree of conjugation of the vinyl junction moiety. A similar argument also holds for the physical meaning of d^R, and an increasing d^R value indicates the formation of a quinoidal structure. The current system has four six-membered rings and three vinyl junctions (R1 and R2 in the D unit and R3, R4, and VJ3 in the A unit), as well as two other vinyl junctions (VJ1 and VJ2). Their different geometries and degrees of conjugation are easily examined with the BLA parameters.

2.2. Electronic-Structure Calculations. The excited states of the SBS system were investigated by TDDFT,[38−43] because it is a practical approach that balances computational efficiency and accuracy. The dependence of the results of excited-state calculations on the functional used was carefully evaluated.

DOI: 10.1021/acs.jpca.5b00354
J. Phys. Chem. A 2015, 119, 6937−6948

After the ground state had been optimized, the vertical excitation energies of the low-lying excited states were calculated using various functionals. Several standard functionals with fixed amounts of Hartree−Fock (HF) exchange were employed, including BP86[44,45] (0% HF), B3LYP[46,47] (20% HF), PBE0[48−50] (25% HF), and BH&HLYP[44,46,51] (50% HF). Based on the BLYP functional,[44,46] several user-defined (UD) functionals with different amounts of HF exchange were also constructed for comparison and were named according to their percentage of HF exchange. For example, the UD50 functional refers to a modified BLYP functional with 50% HF exchange. The range-separated functionals CAM-B3LYP,[52] LC-ωPBE,[53,54] and ωB97XD[55] and the Minnesota functionals M06-2X[56] and M11[57] were also employed because they are generally believed to provide reasonable descriptions of charge-transfer (CT) excited states.[41,58,59] As a complementary comparison, the configuration interaction singles (CIS) and time-dependent Hartree−Fock (TDHF) methods, as well as high-level correlated methods [RICC2,[60] ADC(2),[61,62] and SCS-ADC(2)[61−64]] were also employed. In all calculations with the standard functionals, the CIS and TDHF methods, and the high-level correlated methods, the def2-SVP[65,66] basis set and the Turbomole[67] 6.5 program were used. For all calculations with the user-defined functionals, the range-separated functionals, and the Minnesota functionals,[57,68] the 6-31G* basis set and the Gaussian 09 program[69] were used.

The benchmark calculations showed that most functionals (except for those with a relatively small amount of HF exchange) gave very similar results for the two lowest excited states (S_1 and S_2) that are characterized by two local-excitation (LE) transitions at the D and A units (see the Results section).

2.3. Nonadiabatic Dynamics. The nonadiabatic dynamics simulations were carried out using our homemade package called JADE[30] within the framework of the on-the-fly trajectory surface-hopping (TSH) method. Because all technical details can be found in a previous article,[30] we outline only the relevant theoretical issues here. In the TSH method, a single classical trajectory $\mathbf{R}(t)$, computed by the numerical integration of Newton's equations, is used to describe the nuclear motion on a single surface. The nuclear coordinates are propagated using the velocity Verlet algorithm.[70] The electronic wave function satisfies the time-dependent Schrödinger equation, and the propagation of the quantum amplitudes $[c_j(t)]$ of electronic states along the nuclear trajectory $\mathbf{R}(t)$ can be defined by the following set of coupled differential equations

$$i\frac{\mathrm{d}c_j(t)}{\mathrm{d}t} = \sum_i c_i(t)[H_{ji} - i\mathbf{v}\cdot\mathbf{F}_{ji}] \tag{3}$$

In eq 3, $\mathbf{v}$ is the vector of nuclear velocities, and the electronic Hamiltonian matrix (H_{ji}) and nonadiabatic coupling vector ($\mathbf{F}_{ji}$) between states j and i can be expanded in a set of known electronic bases (ϕ_i) as follows

$$H_{ji} \equiv \langle\phi_j|H_e|\phi_i\rangle \tag{4}$$

$$\mathbf{F}_{ji} \equiv \langle\phi_j|\nabla_R|\phi_i\rangle \tag{5}$$

In our implementation, the solution of eq 3 is obtained by performing a unitary propagation of the quantum amplitudes.[71]

In the adiabatic representation, the electronic wave functions are eigenfunctions of the electronic Hamiltonian. Thus

$$H_{ji} = \varepsilon_i\delta_{ji} \tag{6}$$

Then, the transition probability for jumping from one potential energy (PE) surface to another is evaluated based on Tully's fewest-switches algorithm[25]

$$P_{ij} = \frac{2\Delta t\,\mathrm{Re}(c_i^* c_j)\mathbf{v}\cdot\mathbf{F}_{ji}}{|c_i|^2} \tag{7}$$

The nonadiabatic coupling terms can be reformulated as the scalar product of the velocity vector $\mathbf{v}$ and the nonadiabatic coupling vector $\mathbf{F}_{ji}$[72−78]

$$\sigma_{ji}(t) \equiv \mathbf{v}\cdot\mathbf{F}_{ji} = \left\langle\varphi_j\middle|\frac{\partial}{\partial t}\middle|\varphi_i\right\rangle \approx \frac{\langle\varphi_j(t)|\varphi_i(t+\Delta t)\rangle - \langle\varphi_j(t+\Delta t)|\varphi_i(t)\rangle}{2\Delta t} \tag{8}$$

where Δt is the integration time step. The electronic ground state can be represented by a single Slater determinant built from the occupied Kohn−Sham orbitals, whereas the wave functions for the excited electronic states can be approximated by a CIS-type expansion. In accordance with the Casida assignment ansatz,[43,79] the excited-state CIS-type wave function is constructed from the linear-response TDDFT solutions; thus, the obtained nonadiabatic coupling terms are approximate. Following previous studies,[41,42,72−77,80,81] the excited-state wave function is written as

$$|\Psi_K[\mathbf{r};\,\mathbf{R}(t)]\rangle = \sum_{i,a} c_{i,a}^K|\Phi_{ia}^{CSF}[\mathbf{r};\,\mathbf{R}(t)]\rangle \tag{9}$$

$$c_{i,a}^K = \sqrt{\frac{\varepsilon_a - \varepsilon_i}{\omega_K}}\mathbf{Z}_{i,a}^K \tag{10}$$

where ε_a and ε_i are the energies of virtual and occupied molecular orbitals, respectively. In addition, ω_K is the corresponding excited energy. The vector $\mathbf{Z}$ is given by

$$\mathbf{Z} = (\mathbf{A} - \mathbf{B})^{-1/2}(\mathbf{X} + \mathbf{Y}) \tag{11}$$

where $\mathbf{X}$ and $\mathbf{Y}$ represent the solutions of the TDDFT pesudoeigenvalue problem and $\mathbf{A}$ and $\mathbf{B}$ are standard TDDFT matrices.[41,79]

The advantage of the surface-hopping approach is that it can directly provide real-time molecular motions in nonadiabatic dynamics at the atomic level. However, it is well-known that surface-hopping dynamics at the TDDFT level gives an approximated description of the nonadiabatic dynamics because of the ad hoc approach in Tully's surface-hopping algorithm[25,82−88] and the limitations of linear-response TDDFT.[41] Thus, we must admit that the current dynamics simulations provide only a qualitative description of the physical mechanism of the EET process. In this sense, any functional giving a rational result is a good candidate for the on-the-fly simulations. Because the BH&HLYP functional provides a reasonable description of the low-lying excited states of the SBS system (see the Results section), it was selected for the surface-hopping simulations to obtain physical insight into the EET dynamics. For this purpose, the surface-hopping dynamics was performed with our JADE package,[30] which includes a module to control TDDFT/BH&HLYP/def2-SVP calculations in the Turbomole software.[67]

The time steps were 0.5 and 0.005 fs for nuclear motion and electronic propagation, respectively. The technical details of using different time steps in nuclear propagation and electronic

DOI: 10.1021/acs.jpca.5b00354
J. Phys. Chem. A 2015, 119, 6937−6948

motions are discussed in the Supporting Information. The final results were obtained by averaging 100 trajectories. As is well-known, the standard trajectory surface-hopping method suffers from the overcoherence problem.[82−89] To avoid this issue, the decoherence correction proposed by Granucci and Persico[89] was introduced during the dynamics process with the relevant constant $C = 0.1$. A few previous studies discussed the potential deficiency of TDDFT in the description of the PE surface crossing between the ground and excited states.[90] However; this problem is beyond our consideration because the EET processes in the SBS system occur only as nonadiabatic transitions between different electronically excited states.

In the D unit, the rotation of the CC single bond between R1 and R2 results in two isomers ($\tau_1 > 0$ and $\tau_1 < 0$). On the acceptor side, the existence of the vinyl group (VJ3) also leads to cis/trans conformations. In addition, the different orientations of the two vinyl groups (VJ1 and VJ2) with respect to the $-SiH_2$ group also define different conformations; see examples in Scheme 3. The detailed definitions of these

Scheme 3. Five Isomers (C1−C5) Distinguished by Different Rotations of the Two Vinyl Groups Connecting with the $-SiH_2$ Group

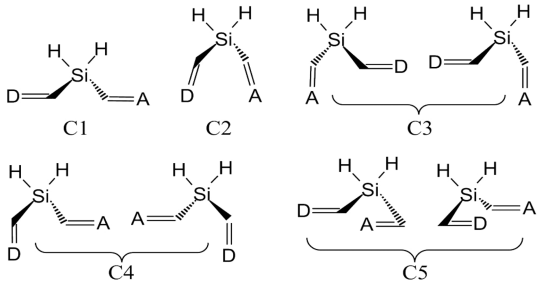

conformations were discussed in previous works[19,20] and are presented in Table S1 (Supporting Information). Furthermore, as noted by Liu et al., many isomers of the SBS system have similar energies (<6 kJ/mol).[20] In this sense, the determination of the initial conditions for nonadiabatic dynamics is quite challenging, because it is not easy to take both multiple minima and their associated velocities into account. In practice, we employed two different initial sampling methods in this work.

The first method was mainly designed to consider many conformations. Because of the large number of isomers distinguished by large distortional coordinates and also possibly separated by large barriers, it is not trivial to include many isomers in the initial sampling. Our test calculations indicated that a long-time molecular dynamics (MD) simulation at room temperature did not sample many isomers because of their separation by high energy barriers. A better sampling approach was employed according to the following procedure: A high-temperature MD run was performed to generate many points in phase space, which were then used as the initial conditions in the subsequent MD run at room temperature. Alternatively, a similar methodology would be to perform Wigner sampling at different S_0 minima. However, with such approaches, an extremely large number of initial conditions would be generated because sufficient sampling points should be produced for each isomer because of their differences in geometry. This results in the propagation of an extremely large number of trajectories, which seems to be impossible with the current on-the-fly approach because of the huge computational cost. Because our purpose was to obtain a rather qualitative understanding of the EET dynamics of many isomers, a rather simplified method was employed in the initial sampling. Born−Oppenheimer molecular dynamics (BOMD) simulations on the ground state were performed at 1000 K at the AM1 level using the MNDO (Modified Neglect of Diatomic Overlap) program.[91] An extremely high temperature of 1000 K was used to generate all possible conformations separated by significant barriers; however, such an unphysically high temperature leads to very strong geometry distortions and extremely large velocities. We checked the trajectory to avoid cleavage of the system. Afterward, 100 randomly selected snapshots from the MD run were taken as the initial guess to perform the ground-state geometry optimization. In this way, we can obtain several ground-state minimum-energy geometries with quite different configurations. Instead of successively generating a large number of sampling points for all minimum-energy geometries, we only considered the coordinates of these minima and neglected the velocity in the starting conditions of the nonadiabatic dynamics simulations. We concede that this approach is rather approximated; however, it should be acceptable for a qualitative understanding of the EET dynamics of the different isomers. This sampling method was named the MD-OPT sampling method. More discussions on the number of isomers and sampled geometries in the MD-OPT method can be found in the Supporting Information (see Tables S1 and S2).

To examine the impact of the velocities on the nonadiabatic dynamics, we also employed the second approach based on the Wigner sampling methodology, denoted as the WST method. In this approach, we considered only one stable configuration (the a-C3-n isomer defined in Table S2, Supporting Information, the so-called cis-anti-anti configuration in Liu et al.'s work[19,20]) as the reference geometry. Then, the initial conditions (geometries and velocities) were generated from the Wigner distribution function of the normal modes of the reference geometry. In this way, both the initial configurations and velocities were reasonably sampled because their correlations and distributions were obtained from the quantum-classical correspondence. Nevertheless, we did not need to address the influence of the various isomers again because the first sampling method was designed for this purpose.

The initial conditions were created by vertically putting all of the snapshots generated by the two sampling methods into the S_2 state (corresponding to the D → D LE excitation). Because the two sampling methods gave consistent results for the intramolecular motions in the nonadiabatic dynamics simulation, we believe that they both captured the main features of the EET process of the SBS system.

2.4. Transition Density Analysis. Analysis of the intramolecular EET process requires the identification of the contributions of two local excitations (D → D and A → A LE) on the involved excited states. We employed the theoretical method based on the single-electron transition density matrix[92,93] for such an analysis. Because this method was explicitly discussed in previous studies,[36,92−96] we outline only the main idea here and provide all of the details in Figure S1 (Supporting Information). The one-electron transition density matrix $T_{EG,[LO]}$ in Löwdin's[92] atomic-orbital basis is obtained as

DOI: 10.1021/acs.jpca.5b00354
J. Phys. Chem. A 2015, 119, 6937−6948

$$\mathbf{T}_{EG,[LO]} = (\mathbf{S}_{[AO]})^{1/2}\mathbf{T}_{EG,[AO]}(\mathbf{S}_{[AO]})^{1/2} = (\mathbf{S}_{[AO]})^{1/2}(\mathbf{C}\mathbf{T}_{EG,[MO]}\mathbf{C}^{T})(\mathbf{S}_{[AO]})^{1/2} \quad (12)$$

where $\mathbf{C}$ is the MO coefficient matrix and $\mathbf{S}_{[AO]}$ is the atomic orbital (AO) overlap matrix. $\mathbf{T}_{EG,[AO]}$ and $\mathbf{T}_{EG,[MO]}$ represent the one-electron transition density matrices between the ground and excited states in the atomic orbital (AO) and molecular orbital (MO) bases, respectively. Because of the orthogonalization of Löwdin's atomic orbitals, the transition contribution between different atoms simply becomes

$$D_{ab}^{EG} = \sum_{i\in a, j\in b} (\mathbf{T}_{EG,[LO]})^2_{ij} \quad (13)$$

where i and j are the indices of the atomic basis and a and b are the indices of atoms. Thus, the transition contribution from fragment D to fragment A of a molecule is given by

$$\Omega_{DA}^{EG} = \sum_{a\in D, b\in A} D_{ab}^{EG} \quad (14)$$

The cases of D = A and D ≠ A in eq 14 represent the LE (D → D and A → A) excitations and the CT (D → A and A → D) excitation components, respectively. In this way, the contributions of all of the LE and CT excitations can be directly obtained for an excited state.

In the transition density analysis, the SBS system was divided into three parts: the donor part (D), the $-SiH_2$ moiety, and the acceptor part (A). Accordingly, we easily obtained the different LE contributions (D → D or A → A) for an excited state. In particular, the time-dependent LE evolution during the nonadiabatic dynamics simulations should directly reflect the intramolecular D—A EET process.

3. RESULTS

3.1. Ground and Excited States. As discussed in a previous work, the SBS system has many conformations with minor energy differences.[20] A similar conclusion was also reached with our MD-OPT sampling process. More details concerning the geometries sampled with the MD-OPT method are given in the Supporting Information (see Tables S1 and S2). Because the two sampling methodologies gave essentially the same internal molecular motions in the EET dynamics, we considered only one stable configuration (the a-C3-n isomer defined in Table S2, Supporting Information, the so-called cis-anti-anti configuration in Liu et al.'s work[19,20]) as the reference example to explain the basic features of the ground and excited states of the SBS system. A similar ground-state minimum of this reference configuration was obtained at both the B3LYP/def2-SVP and BH&HLYP/def2-SVP levels, implying the weak dependence of the ground state on the functional. At this selected reference geometry, the D and A moieties displayed different geometrical features. In the D unit, the distance r and twisting angle τ_1 of the CC bond between R1 and R2 were found to be 1.48 Å and 36°, respectively (Figure 1a). In the A unit, the two rings (R3 and R4) and VJ3 were all found to lie in the same plane (Figure 1b). Overall, the D and A units can be treated as two π-conjugated systems separated by the $-SiH_2$ moiety.

At the ground-state minimum of the reference geometry, the low-lying excited states were calculated using different methods (TDHF, CIS, and TDDFT). The vertical excitation energies for the lowest D → D (LE), A → A (LE), and D → A (CT) states

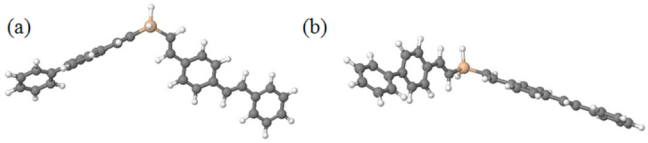

Figure 1. Two views of the ground-state structure for the reference configuration of the SBS system.

are depicted in Figure 2, and more details can be found in Tables S3 and S4 (Supporting Information).

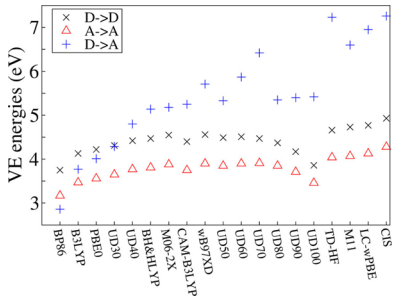

Figure 2. Vertical excitation (VE) energies (eV) for the two lowest LE states (D → D and A → A) and the lowest CT state (D → A) using the TDDFT method with a series of functionals, the TDHF method, and the CIS method.

Most functionals gave consistent results for the energy gap of the two lowest LE (D → D and A → A) states, although a few functionals including UD90 and UD100 gave a smaller energy gap between the two lowest LE states. This indicates that the relative energies of the two LE states are not strongly dependent on the method. However, the energy of the first D → A CT state was highly modified by the different amounts of HF exchange. For the functionals with very small amounts of HF exchange, such as BP86 (0%), B3LYP (20%), PBE0 (25%), and UD30 (30%), the CT state was significantly underestimated and was even lower than the D → D transition. This artifact was easily identified because all of the range-separated functionals, which were expected to give better results for the CT state, showed that the CT state was always higher than the D → D transition. When an adequate amount of HF exchange was included, the D → D and A → A transitions were lower than the CT state, avoiding the CT problem. Most importantly, a few functionals such as BH&HLYP, CAM-B3LYP, ωB97XD, M06-2X, and UD50-UD80 gave reasonable and consistent results. The spectra computed using the BH&HLYP and CAM-B3LYP functionals with the WST method (Figure 3 and Figure S2, Supporting Information) are similar to the available experimental spectra of the $(DA)_m$ system.[20]

Four frontier orbitals (from HOMO − 1 to LUMO + 1, where HOMO and LUMO represent the highest occupied molecular orbital and lowest unoccupied molecular orbital, respectively) obtained at the BH&HLYP/def2-SVP level are shown in Figure 4. HOMO − 1 and LUMO + 1 are located on the D unit, whereas HOMO and LUMO are located on the A unit. The S_1 and S_2 states are mainly characterized by the HOMO → LUMO and HOMO − 1 → LUMO + 1 transitions, respectively. Thus, S_1 and S_2 are well-described by the A → A and D → D LE transitions, respectively. The character assignment of S_1 and S_2 remained the same for all functionals with a reasonable amount of HF exchange, such as BH&HLYP, CAM-B3LYP, ωB97XD, M06-2X, and UD50-UD80. The

DOI: 10.1021/acs.jpca.5b00354
J. Phys. Chem. A 2015, 119, 6937−6948

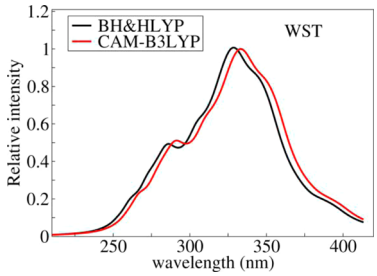

Figure 3. Simulated absorption spectra of the SBS system in the gas phase obtained using the BH&HLYP and CAM-B3LYP functionals with the WST sampling method.

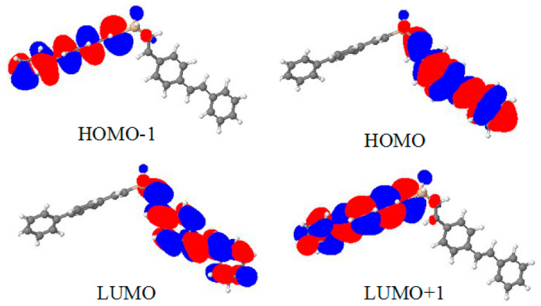

Figure 4. Frontier orbitals (from HOMO − 1 to LUMO + 1) of the optimized ground-state minimum for the SBS system.

transition density analysis also provided a clear picture of the two LE excitation characters for the S_1 and S_2 states (Figure S1, Supporting Information). Therefore, the D and A units can be considered as independent fragments at the Franck−Condon (FC) region. Although the vertical excitation energies for S_1 and S_2 obtained by TDDFT calculations with reasonable functionals were higher than the experimental results based on the absorption spectra of the D and A units, the calculated S_1−S_2 energy gap was still reasonable.

Considering that the BH&HLYP functional gave a reasonable description of the two lowest excited states and relevant absorption spectra, it was considered acceptable to apply this functional to the D—A EET dynamics of the SBS system.

3.2. Nonadiabatic Dynamics. With both sampling methods (MD-OPT and WST), an ultrafast decay to the S_1 state was observed after the initial excitation to the S_2 state (Figure 5). In the MD-OPT sampling, more than 50% of the trajectories jumped from the S_2 state to the S_1 state within 70 fs, and the S_2—S_1 internal conversion was essentially complete within 200 fs. The dynamics with the WST sampling gave a

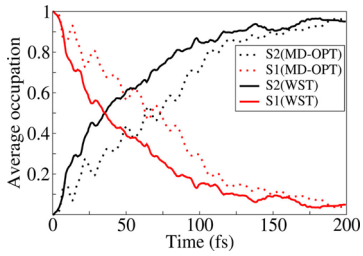

Figure 5. Time-dependent average fractional occupation of the two excited states S_1 and S_2 as obtained with the MD-OPT method (dotted line) and the WST method (solid line).

faster S_2—S_1 population transfer. Such a difference is easily explained by the fact that the initial velocities were assigned as zero and nonzero in the MD-OPT and WST sampling methods, respectively. Thus, the latter case could lead to rapid access to the S_1—S_2 crossing (or avoided crossing) region and faster population decay. Because the S_1 and S_2 states are dominated by the A → A and D → D LE excitations, respectively, we expect that S_2—S_1 decay is highly responsible for the intramolecular D—A EET process of the SBS system. The decay in the current simulations seems to be faster than the previous experimental result (~300 fs) obtained on the basis of time-resolved spectroscopy and theoretical estimations.[19,20] One possible reason for the difference is that the system in the current study is a model of the SBS system, whereas the realistic systems in the experimental work consisted of $(DA)_m$ or $(D_3A)_m$ copolymers in solutions of *p*-dioxane, tetrahydrofuran (THF), CH_2Cl_2, and $CHCl_3$. In principle, the steric hindrance arising in the polymer and the viscosity of the solvent lead to slower nuclear motions and longer decay time scales.

To provide a more direct representation of the EET process, we also evaluated the time-dependent transition density in the nonadiabatic dynamics. As discussed previously, the SBS system was divided into three parts: the D unit, the $-SiH_2$ moiety, and the A unit. The time-dependent D → D and A → A LE transition densities (averaged over 19 trajectories) using the WST method are presented in Figure 6.

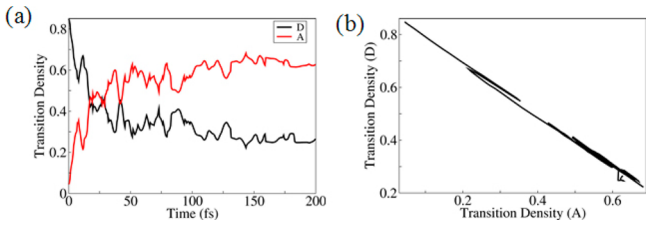

Figure 6. (a) Time-dependent D → D and A → A LE transition densities obtained using the WST method (averaged over 19 trajectories) within 200 fs; (b) evolution of these two LE transitions with time.

Because the initial state S_2 is mainly characterized by the HOMO − 1 → LUMO + 1 transition, the transition density analysis indicates that the D → D LE transition is dominant (>80%) at the beginning of the dynamics whereas the A → A LE transition plays only a minor role (approximately 5%). Other components, such as the LE excitation on the $-SiH_2$ moiety and the weak CT excitation among the different units, are less important. Within the initial 20 fs, the D → D LE transition decreased quickly as the A → A LE transition increased simultaneously. From 20 to ~50 fs, oscillatory patterns of the D → D and A → A LE components were observed, reflecting the fact that the trajectories were travelling in the strong interstate coupling region with a significant mixture of different electronic characters. Later in the simulation, the contribution of the A → A LE transition became increasingly dominant, implying the termination of the EET process. Interestingly, the time-correlated evolution trajectory of the two LE transitions in Figure 6b is linear and has a slope close to 1, indicating that the sum of the two LE transitions should be a constant. In other words, all other transition components were not important for the current EET

DOI: 10.1021/acs.jpca.5b00354
J. Phys. Chem. A 2015, 119, 6937−6948

process, considering that the initial configuration was mainly governed by the D → D LE transition.

To explore the active coordinates responsible for the S_2—S_1 decay dynamics, the internal coordinates were checked at the initial time and at the S_2—S_1 hoping events for all trajectories. The distributions of relevant geometrical parameters are given in Table S5 and Figures S3–S6 (Supporting Information), and only the photoactive key coordinates are discussed here (Figure 7). In the WST sampling approach, geometry alternation of the

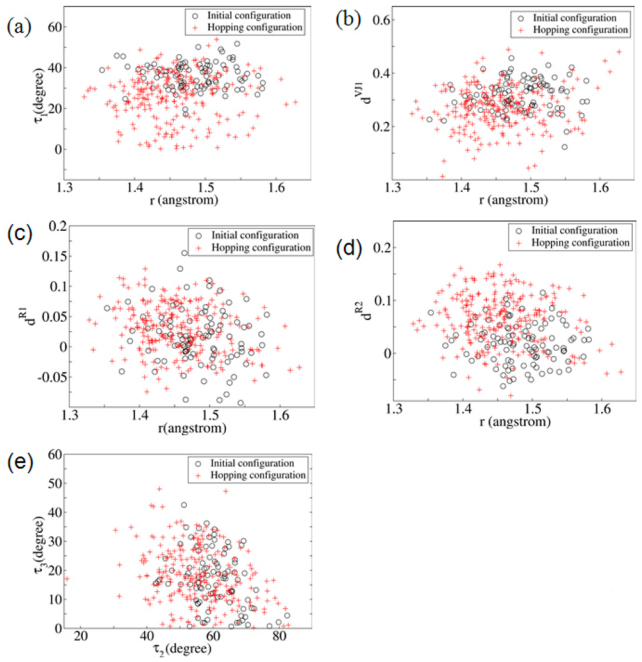

Figure 7. Two-dimensional distributions of the internal coordinates at the initial and hopping configurations: (a) r–τ_1, (b) r–d^{VJ1}, (c) r–d^{R1}, (d) r–d^{R2}, and (e) τ_2–τ_3.

D moiety was observed during the S_2—S_1 decay, whereas the A moiety remained essentially unchanged. The most significant variation occurred at the CC bond connecting the two six-membered rings R1 and R2 (Figure 7a). From time zero to the hopping events, both the CC bond length r and the relevant dihedral angle decreased obviously (Figure 7a). We also observed that the hops occurred within the large area described by the torsional angle τ_1. This strongly indicates that enhanced planarity of the D moiety is mainly responsible for the S_2—S_1 decay. However, the D moiety did not become fully planar during the S_2—S_1 hops, possibly because of the steric effects between the two adjacent H atoms of R1 and R2. In addition, the two six-membered rings and the vinyl junction also experienced an obvious in-plane deformation, reflected by the BLA parameters (R1, R2, and VJ1) of the D moiety. The variations of the BLA parameters for the rings (R1 and R2) and VJ1 from time zero to the hopping events are given in Figure 7b–d. For R1 and R2, the values of the BLA parameters increased, implying a decrease in the degree of conjugation with the change from the aromatic to the quinoidal structure. However, the degree of conjugation of the entire D unit should increase because of the shortening CC bond between R1 and R2. The values of the BLA parameters for VJ1 decreased, also indicating the increasing degree of conjugation in the VJ1 unit. Thus, the overall conjugation of the D unit should be enhanced. In contrast, only very minor geometrical changes were observed in the A moiety during S_2—S_1 nonadiabatic decay.

It should be noticed that the orientations of the D and A units changed simultaneously because of the repulsive interaction between the two branches, and this coupled motion is clearly characterized by the strong correlation between τ_2 and τ_3. (Figure 7e). However, such a coupled motion between D and A is not relevant to the EET dynamics because no significant differences appeared in the two-dimensional distributions of τ_2 and τ_3 between the initial conditions and the hopping events.

The enhancement of the overall degree of conjugation in the D unit is critical for the intramolecular EET process, whereas the geometry of the A unit remains basically unchanged. The underlying reason seems obvious. One can treat the D and A units as two individual segments that have different sets of local orbitals. The increasing overall degree of conjugation in the D unit causes the energy of the localized occupied orbitals to increase and that of the localized unoccupied orbitals to decrease, further reducing the D → D LE transition energy. At the same time, the A segment and its relevant localized orbitals remain almost unchanged. When the D → D LE transition energy becomes close to the A → A LE transition energy, the efficient D—A EET process becomes highly possible.

Although different time scales were observed for the MD-OPT sampling method and the WST method, the two methods gave similar molecular motions. The differences in the results obtained with these two methods should certainly be mentioned. The MD-OPT sampling included many conformations with different ranges of the R1–R2 twisting angles, whereas only one twisting possibility existed for τ_1 in the WST sampling. Thus, the distribution of the dihedral angle τ_1 displays two peaks in the MD-OPT sampling (see Figure S3, Supporting Information) but only one in the WST sampling. In the MD-OPT sampling, the distribution of the initial conformations was more localized because all of the initial conformations were generated after ground-state optimization. This explains why the peaks at time zero in the MD-OPT method were sharper than those in the WST sampling.

The evolution of the important internal coordinates—namely, dihedral angles (τ_1) and relevant CC bond lengths (r)—with the total simulation time of the trajectories in the WST method are given in Figure 8. An obvious oscillation pattern of r with a period of 18 fs was observed in the dynamics process, in which the distribution of r was within the range 1.4–1.5 Å. The dihedral angle τ_1 started at its initial value and then decreased continuously, indicating that the D moiety became more planar. Interestingly, the center of the τ_1

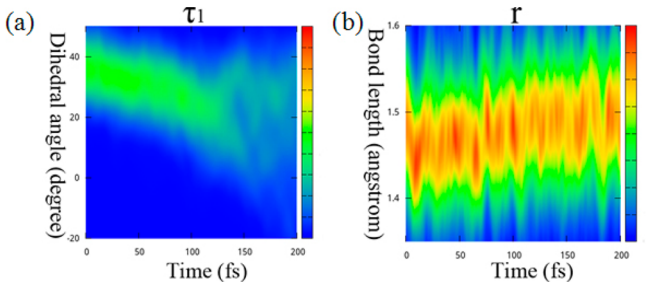

Figure 8. Geometrical distributions of (a) dihedral angle τ_1 and (b) bond length r with time over all configurations in 100 trajectories using the WST method.

DOI: 10.1021/acs.jpca.5b00354
J. Phys. Chem. A 2015, 119, 6937–6948

distribution at 50 fs was approximately 29°, consistent with the hopping distributions (Figure 7a and Figure S3, Supporting Information). Overall, it is highly plausible that the system might first experience the shortening motion of r and then the relevant torsional motion to access the S_1—S_2 crossing (or avoided crossing) region. After ∼100 fs, the distribution of τ_1 started to bifurcate, implying that the twisting motions might follow either the forward or backward pathways. The presence of this bifurcated feature is reasonable because the rotation of the dihedral angle τ_1 can occur in two possible directions.

The D—A EET process is basically governed by the excited-state dynamics of the D unit, which involves the shortening of the CC bond length, the reduction of the torsional dihedral angle between the two phenyl groups, and the formation of quinoidal structures. Similar motions were also identified as the leading features in the excited-state dynamics of a D derivative.[97] Previous experimental measurements and theoretical calculations indicated that the vibrational relaxation dynamics on the excited state of the D derivative leads to the transformation of R1 and R2 from an aromatic structure to a quinoidal structure,[98,99] consistent with the time-dependent behavior of their BLA parameters (Figure S7, Supporting Information) in our nonadiabatic dynamics simulations. Moreover, we also found that the length of the CC bond (between R1 and R2) and the BLA parameter of R2 displayed similar oscillations with an ∼18 fs period, which might be responsible for the phenyl C═C stretching (∼1700 cm^{-1}), as reported in previous published works.[14,100]

To obtain a more intuitive picture of the EET dynamics, the time-dependent energy difference, electronic character (assigned by transition density), and internal coordinates for a representative trajectory are plotted in Figure 9. More plots of this trajectory can be found in Figure S8 (Supporting Information). From this typical trajectory, several $S_2 \rightarrow S_1$ transitions and the corresponding reverse hops can be observed that take place for geometries with an S_1−S_2 energy difference of approximately 0.25−0.3 eV. A similar behavior was observed for other trajectories as well. Thus, it is highly possible that the S_1—S_2 avoided crossing, instead of the conical intersection, plays an essential role here, which is consistent with the profiles of the PE surfaces (see below). The evolution of the electronic character (assigned by the transition density) indicates that strong oscillations occur between the D and A units before 100 fs. When the trajectory finally decays into the S_1 state, such oscillations vanish, and the EET dynamics is completed.

During the entire dynamics simulation, the sum of the D−D and A−A transitions was always ∼90%, indicating weak contributions from other transitions. The evolution of the important internal coordinates for this representative trajectory is given in Figure 9c−f. Clearly, most hops take place for geometries with shorter r and smaller τ_1. In addition, the torsional motion of τ_1 takes place later in time than the very rapid oscillation of the bond length r. The evolutions of r, τ_1, and the BLA parameters (R2 and VJ1) are coupled with each other. All of the evolutions in this typical trajectory are consistent with the corresponding dynamics features over all of the trajectories (Figures 7 and 8).

3.3. Reaction Mechanism of the EET Process. After the discussion of the EET dynamics, it should be useful to re-examine the excited-state reaction pathway in detail and obtain a clear picture of the active molecular motions involved in such EET processes. Scans of the critical geometries along the major reactive coordinates of the S_1 and S_2 PE surfaces, from the FC region to the hopping region, were performed using the BH&HLYP functional and the ADC(2) method. We divided the PE surface scans into two steps. First, the constrained optimization of the S_2 state was performed by fixing τ_1 = 40° because this value is close to the torsion angle of the two six-membered rings at the FC region. A linear interpolation was used to connect the PE surfaces from the FC region to the obtained optimized geometry with τ_1 = 40°. Because the bond length r is the active coordinate during such an optimization, it was used as the primary reactive coordinate to represent the PE surface scan. Second, a relaxed S_2 scan was conducted with the constrained dihedral angle τ_1 varying from −10° to 40°. The results are collected in Figure 10.

At the BH&HLYP level, the decrease in r significantly induced the drop of the S_2 energy at fixed τ_1 = 40°, whereas the

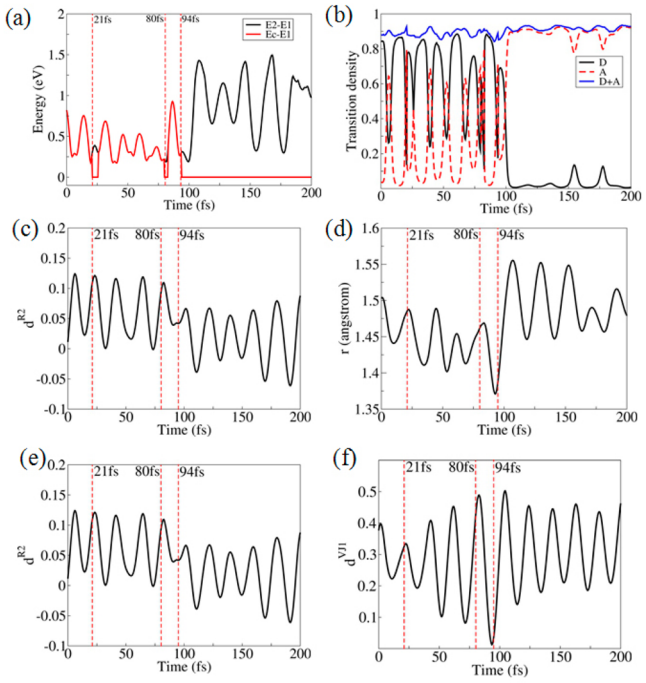

Figure 9. (a) Time-dependent difference in the energies of two states (S_2 and the current state with respect to the S_1 state) in a representative trajectory. (b) Time-dependent D → D and A → A LE transition densities and their sum. (c−f) Evolutions of the internal coordinates (c) r, (d) τ_1, (e) d^{R2}, and (f) d^{VJ1} for a representative trajectory of 200 fs. The S_2−S_1 hops occur at 21, 80, and 94 fs.

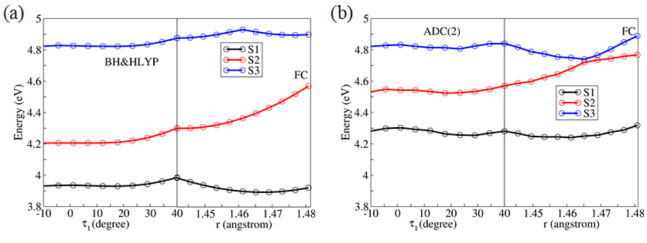

Figure 10. PE surfaces of the three lowest excited states (S_1, S_2, and S_3). A linear interpolation is used to connect the PE surfaces between the FC region and the geometry obtained from the constrained optimization (τ_1 = 40°); see right sides of panels a and b. We used the bond length r as the primary coordinate to represent the x axis of the rigid PE surface scan. A relaxed S_2 scan was conducted with the constrained dihedral angle τ_1 varying from −10° to 40°. The results were obtained at two levels: (a) BH&HLYP and (b) ADC(2).

DOI: 10.1021/acs.jpca.5b00354
J. Phys. Chem. A 2015, 119, 6937−6948

S_1 energy changed only slightly. As a result, the S_1-S_2 energy gap decreased from ~0.6 to ~0.3 eV. Afterward, when τ_1 was varied from 40° to −10°, the S_1-S_2 energy gap still decreased. Both the S_1 and S_2 PE surfaces became rather flat when τ_1 was less than 25° and when the S_1-S_2 energy gap was between 0.25 and 0.3 eV. All efforts to search for the geometry at the real S_1-S_2 PE crossing were in vain. Thus, the S_1-S_2 avoided crossing, instead of the conical intersection, should be responsible for the nonadiabatic EET dynamics of the current system.

The PE profiles in Figure 10a clearly show a few important features of the EET dynamics. At the beginning of the EET dynamics, the S_2 energy decreases dramatically when r decreases. During this process, the BLA parameters of the D unit, such as R1, R2, and VJ1, also change obviously. Afterward, τ_1 becomes smaller, and the system tends to become more "planar". This motion drives the system into the S_1-S_2 avoided crossing region with very flat S_1 and S_2 PE surfaces. Then, the system resides in this region for dozens of femtoseconds and experiences several hops before the trajectory finally decays to the S_1 state. Between these hopping events, we expect that the r stretching motion can push the system close to or away from the S_1-S_2 avoided crossing region, inducing forward and backward D—A EET. The evolution of r should be highly correlated with the BLA of all of the conjugated units. All of these features are consistent with the behavior of a typical trajectory and with the distribution of the hopping geometries.

It should be highly interesting to employ high-level correlated electronic methods for a complementary physical insight into the EET dynamics of the SBS system. The excitation energies (in eV), oscillator strengths (OSs), and transition contributions of the three lowest excited states (S_1, S_2, and S_3) in the FC region of the SBS system were obtained using the ADC(2)/def2-SVP, RICC2/def2-SVP, and SCS-ADC(2)/def2-SVP methods (Table S7, Supporting Information). At first glance, the results obtained at these levels did not seem fully consistent with the data obtained at the TDDFT level. For example, these correlated electronic methods showed that S_2 and S_3 are dominant for the A → A and D → D transitions, respectively, whereas the reverse assignment was observed in all TDDFT calculations. We noticed that previous works on organic photovoltaic compounds[96,101] also observed a similar situation. However, this difference might not influence the active intramolecular motion in the EET dynamics of the SBS system if the reactive coordinates of the PE surfaces are considered.

Because the ADC(2)/def2-SVP, RICC2/def2-SVP, and SCS-ADC(2)/def2-SVP methods gave very similar results for the vertical excitation energies in the FC region, we employed only the ADC(2) method to construct the excited-state PE surfaces (Figure 10b). Although the ADC(2) method gave a different ordering of the S_2 and S_3 states in the FC region, the state with the D → D transition dropped very rapidly and the S_2 state quickly changed character for r < 1.47 (Figure 10b). Because the large gradient driving the decrease in r exists on the S_3 state (the FC region) and at the S_2/S_3 crossing, we expect that the system would follow the gradient, experience the decrease in r, and quickly jump to the S_2 state. This process should follow the diabatic pathway that retains the major electronic character of the D → D transition. After this transition, ADC(2) and TDDFT gave very similar results for the S_1 and S_2 states, in terms of both their PE profiles and electronic characters (Figure 10). Thus, these two methods should predict similar reactive coordinates for the EET dynamics, although they give different results in the FC region.

It is also true that one should not neglect the difference between the results derived from the TDDFT and ADC(2) calculations. Certainly, we cannot deny that the second A → A excited state might be involved in the EET dynamics if the nonadiabatic dynamics simulations were run at the ADC(2) level. However, without further evidence, it is very hard to determine whether the ADC(2) method really provides a better description of the current system than the TDDFT method with a suitable functional. To obtain a very precise picture of the excited-state dynamics of the SBS system, extensive benchmark calculations and nonadiabatic dynamics simulations with other high-level methods are required, and these tasks represent the great challenges of the future. However, the above discussion has clarified that the two methods predict very similar internal molecular motions in the EET dynamics. In particular, because the CT state is not involved at all, the TDDFT method with a suitable functional should, in principle, provide an acceptable description of the EET dynamics involving only valence excitations. In addition, a significant double-excitation character does not exist in the lowest three excited states (Table S7, Supporting Information); thus, it should be safe to use a single reference method to treat the excited-state dynamics. In this sense, we still believe that the physical mechanism of the EET dynamics, particularly the active internal molecular motions, derived from the on-the-fly surface-hopping simulation at the TDDFT/BH&HLYP level should be reliable, at least at a qualitative level.

4. CONCLUSIONS

In summary, the ultrafast intramolecular excitonic energy transfer from vinylbiphenyl to vinylstilbene in the SBS system was investigated by nonadiabatic dynamics simulations with an on-the-fly surface-hopping method at the TDDFT level. Careful calculations of the low-lying excited states of the SBS system using different electronic-structure methods were carried out. Most functionals with reasonable amounts of HF exchange were found to give very similar results, suggesting that the first two electronic states (S_1 and S_2) are characterized by the A → A LE and D → D LE transitions, respectively.

Nonadiabatic dynamics simulations at the BH&HLYP level showed an ultrafast S_2—S_1 decay that is responsible for the D—A EET process. The evolution of the transition density provides an intuitive picture of such an intramolecular EET process. The geometric changes in the D unit play a very important role, which includes the shortening of the CC bond between R1 and R2, the reduction of the twisting angle between R1 and R2, the aromatic → quinoidal geometry transformation of R1 and R2, and the conjugation enhancement of the VJ1 moiety. In general, these nuclear motions should improve the overall degree of conjugation of the D moiety, whereas the A acceptor unit remains basically unchanged during the EET process. The present work offers a time-dependent perspective on the ultrafast intramolecular EET of the SBS system, which should provide a very useful view toward understanding the more complicated excited-state processes that occur in silylene-spaced conjugated polymers or other similar organic photovoltaic copolymers.

DOI: 10.1021/acs.jpca.5b00354
J. Phys. Chem. A 2015, 119, 6937−6948

■ ASSOCIATED CONTENT

Supporting Information

Molecular geometry, propagation of nuclear and electronic motions with different time steps in surface-hopping calculations, isomers and initial sampling, transition density analysis, vertical excitation energies and calculated absorption spectra, distributions of all relevant geometrical parameters at the initial time and the hopping time, distributions of geometric parameters with time, typical trajectory and comparison of the BH&HLP and ADC(2) methods. The Supporting Information is available free of charge on the ACS Publications website at DOI: 10.1021/acs.jpca.5b00354.

■ AUTHOR INFORMATION

Corresponding Author

*Fax: +86-532-80662778. Tel.: +86-532-80662630. E-mail: lanzg@qibebt.ac.cn.

Author Contributions

The manuscript was written with contributions from all authors. All authors have given approval to the final version of the manuscript.

Funding

This work was supported by the CAS 100 Talent Project, the NSFC project (Grants 21103213 and 91233106), the Key Lab of Nanodevices and Nanoapplications, CAS (14HZ03), and the Director Innovation Foundation of CAS-QIBEBT.

Notes

The authors declare no competing financial interest.

■ ACKNOWLEDGMENTS

The authors thank the Supercomputing Center, Computer Network Information Center, CAS; the National Supercomputing Center in Shenzhen; and the Super Computational Center of CAS-QIBEBT for providing computational resources.

■ REFERENCES

(1) Wang, H. W.; Cheng, Y. J.; Chen, C. H.; Lim, T. S.; Fann, W.; Lin, C. L.; Chang, Y. P.; Lin, K. C.; Luh, T. Y. Photoinduced Electron Transfer in Silylene-Spaced Copolymers Having Alternating Donor−Acceptor Chromophores. *Macromolecules* **2007**, *40*, 2666−2671.

(2) Jung, S. H.; Kim, H. K.; Kim, S. H.; Kim, Y. H.; Jeoung, S. C.; Kim, D. Palladium-Catalyzed Direct Synthesis, Photophysical Properties, and Tunable Electroluminescence of Novel Silicon-Based Alternating Copolymers. *Macromolecules* **2000**, *33*, 9277−9288.

(3) Luh, T. Y.; Cheng, Y. J. Alternating Divinylarene−Silylene Copolymers. *Chem. Commun.* **2006**, 4669−4678.

(4) Yang, D. D. H.; Yang, N. C. C.; Steele, I. M.; Li, H.; Ma, Y. Z.; Fleming, G. R. Photochemistry of Dianthrylsilanes: A Study of σ, π^*-Interaction. *J. Am. Chem. Soc.* **2003**, *125*, 5107−5110.

(5) Brouwer, H. J.; Krasnikov, V. V.; Hilberer, A.; Hadziioannou, G. Blue Superradiance from Neat Semiconducting Alternating Copolymer Films. *Adv. Mater.* **1996**, *8*, 935−937.

(6) Cheng, Y.-J.; Luh, T.-Y. Synthesis, Light-Harvesting and Energy-Transfer Properties of Regioregular Silylene-Spaced Alternating $[(\text{Donor}-\text{SiMe}_2^-)_{n=1-3}-(\text{Acceptor}-\text{SiMe}_2)]$ Copolymers. *Chem.—Eur. J.* **2004**, *10*, 5361−5368.

(7) Saini, S.; Srinivas, G.; Bagchi, B. Distance and Orientation Dependence of Excitation Energy Transfer: From Molecular Systems to Metal Nanoparticles. *J. Phys. Chem. B* **2009**, *113*, 1817−1832.

(8) Hsu, C. P.; You, Z. Q.; Chen, H. C. H. Characterization of the Short-Range Couplings in Excitation Energy Transfer. *J. Phys. Chem. C* **2008**, *112*, 1204−1212.

(9) Lee, T.; Song, K. H.; Jung, I.; Kang, Y.; Lee, S. H.; Kang, S. O.; Ko, J. Silylene-Spaced Diphenylanthracene Derivatives as Blue-Emitting Materials. *J. Org. Chem.* **2006**, *691*, 1887−1896.

(10) Hennebicq, E.; Pourtois, G.; Scholes, G. D.; Herz, L. M.; Russell, D. M.; Silva, C.; Setayesh, S.; Grimsdale, A. C.; Müllen, K.; Brédas, J.-L.; Beljonne, D. Exciton Migration in Rigid-Rod Conjugated Polymers: An Improved Förster Model. *J. Am. Chem. Soc.* **2005**, *127*, 4744−4762.

(11) Cheng, Y. J.; Luh, T. Y. Synthesis and Efficient Energy Transfer in a Three-Chromophore Energy Gradient of Regioregular Silylene-Spaced Divinylarene Copolymers. *Macromolecules* **2005**, *38*, 4563−4568.

(12) Wong, K. F.; Bagchi, B.; Rossky, P. J. Distance and Orientation Dependence of Excitation Transfer Rates in Conjugated Systems: Beyond the Förster Theory. *J. Phys. Chem. A* **2004**, *108*, 5752−5763.

(13) Schwartz, B. J. Conjugated Polymers as Molecular Materials: How Chain Conformation and Film Morphology Influence Energy Transfer and Interchain Interactions. *Annu. Rev. Phys. Chem.* **2003**, *54*, 141−172.

(14) Tretiak, S.; Saxena, A.; Martin, R. L.; Bishop, A. R. Conformational Dynamics of Photoexcited Conjugated Molecules. *Phys. Rev. Lett.* **2002**, *89*, 097402.

(15) Beljonne, D.; Pourtois, G.; Silva, C.; Hennebicq, E.; Herz, L. M.; Friend, R. H.; Scholes, G. D.; Setayesh, S.; Mullen, K.; Bredas, J. L. Interchain vs. Intrachain Energy Transfer in Acceptor-Capped Conjugated Polymers. *Proc. Natl. Acad. Sci. U.S.A.* **2002**, *99*, 10982−10987.

(16) Schultze, X.; Serin, J.; Adronov, A.; Frechet, J. M. J. Light Harvesting and Energy Transfer in a Ruthenium−Coumarin-2 Copolymer. *Chem. Commun.* **2001**, 1160−1161.

(17) Adronov, A.; Robello, D. R.; Frechet, J. M. J. Light Harvesting and Energy Transfer within Coumarin-Labeled Polymers. *J. Polym. Sci. A: Polym. Chem.* **2001**, *39*, 1366−1373.

(18) Fujitsuka, M.; Cho, D. W.; Ohshita, J.; Kunai, A.; Majima, T. Fluorescence Properties of Si-Linked Oligothiophenes. *J. Phys. Chem. C* **2007**, *111*, 1993−1998.

(19) Liu, K. L.; Lee, S. J.; Chen, I. C.; Hsu, C. P.; Chen, C. H.; Luh, T. Y. Ultrafast Energy Transfer in Divinylbiphenyl and Divinylstilbene Copolymers Bridged by Silylene. *J. Phys. Chem. C* **2013**, *117*, 64−70.

(20) Liu, K. L.; Lee, S. J.; Chen, I. C.; Hsu, C. P.; Yeh, M. Y.; Luh, T. Y. Ultrafast Energy Transfer in a Regioregular Silylene-Spaced Copolymer. *J. Phys. Chem. C* **2010**, *114*, 13909−13916.

(21) Förster, T. Zwischenmolekulare Energiewanderung und Fluoreszenz. *Ann. Phys.* **1948**, *2*, 55−75.

(22) May, V.; Kühn, O. *Charge and Energy Transfer Dynamics in Molecular Systems*; John Wiley & Sons: New York, 2008.

(23) Tretiak, S.; Mukamel, S. Density Matrix Analysis and Simulation of Electronic Excitations in Conjugated and Aggregated Molecules. *Chem. Rev.* **2002**, *102*, 3171−3212.

(24) Raychaudhuri, S.; Shapir, Y.; Chernyak, V.; Mukamel, S. Excitonic Funneling in Extended Dendrimers with Nonlinear and Random Potentials. *Phys. Rev. Lett.* **2000**, *85*, 282−285.

(25) Tully, J. C. Molecular Dynamics with Electronic Transitions. *J. Chem. Phys.* **1990**, *93*, 1061−1071.

(26) Barbatti, M.; Granucci, G.; Persico, M.; Ruckenbauer, M.; Vazdar, M.; Eckert-Maksic, M.; Lischka, H. The On-the-Fly Surface-Hopping Program System Newton-X: Application to ab Initio Simulation of the Nonadiabatic Photodynamics of Benchmark Systems. *J. Photochem. Photobiol. A* **2007**, *190*, 228−240.

(27) Fabiano, E.; Keal, T.; Thiel, W. Implementation of Surface-Hopping Molecular Dynamics Using Semiempirical Methods. *Chem. Phys.* **2008**, *349*, 334−347.

(28) Nelson, T.; Fernandez-Alberti, S.; Roitberg, A. E.; Tretiak, S. Nonadiabatic Excited-State Molecular Dynamics: Modeling Photophysics in Organic Conjugated Materials. *Acc. Chem. Res.* **2014**, *47*, 1155−1164.

(29) Barbatti, M.; Ruckenbauer, M.; Plasser, F.; Pittner, J.; Granucci, G.; Persico, M.; Lischka, H. Newton-X: A Surface-Hopping Program

DOI: 10.1021/acs.jpca.5b00354
J. Phys. Chem. A 2015, 119, 6937−6948

for Nonadiabatic Molecular Dynamics. *WIREs Comput. Mol. Sci.* **2014**, *4*, 26−33.
(30) Du, L.; Lan, Z. An On-the-Fly Surface-Hopping Program JADE for Nonadiabatic Molecular Dynamics of Polyatomic Systems: Implementation and Applications. *J. Chem. Theory Comput.* **2015**, *11*, 1360−1374.
(31) Nelson, T.; Fernandez-Alberti, S.; Chernyak, V.; Roitberg, A. E.; Tretiak, S. Nonadiabatic Excited-State Molecular Dynamics Modeling of Photoinduced Dynamics in Conjugated Molecules. *J. Phys. Chem. B* **2011**, *115*, 5402−5414.
(32) Akimov, A. V.; Prezhdo, O. V. Nonadiabatic Dynamics of Charge Transfer and Singlet Fission at the Pentacene/C_{60} Interface. *J. Am. Chem. Soc.* **2014**, *136*, 1599−1608.
(33) Jailaubekov, A. E.; Willard, A. P.; Tritsch, J. R.; Chan, W.-L.; Sai, N.; Gearba, R.; Kaake, L. G.; Williams, K. J.; Leung, K.; Rossky, P. J.; Zhu, X.-Y. Hot Charge-Transfer Excitons Set the Time Limit for Charge Separation at Donor/Acceptor Interfaces in Organic Photovoltaics. *Nat. Mater.* **2013**, *12*, 66−73.
(34) Huang, J.; Du, L.; Wang, J.; Lan, Z. Photoinduced Excited-State Energy-Transfer Dynamics of a Nitrogen-Cored Symmetric Dendrimer: From the Perspective of the Jahn−Teller Effect. *J. Phys. Chem. C* **2015**, *119*, 7578−7589.
(35) Sterpone, F.; Rossky, P. J. Molecular Modeling and Simulation of Conjugated Polymer Oligomers: Ground and Excited State Chain Dynamics of PPV in the Gas Phase. *J. Phys. Chem. B* **2008**, *112*, 4983−4993.
(36) Panda, A. N.; Plasse, F.; Aquino, A. J. A.; Burghardt, I.; Lischka, H. Electronically Excited States in Poly(*p*-phenylenevinylene): Vertical Excitations and Torsional Potentials from High-Level ab Initio Calculations. *J. Phys. Chem. A* **2013**, *117*, 2181−2189.
(37) Lukes, V.; Solc, R.; Barbatti, M.; Elstner, M.; Lischka, H.; Kauffmann, H. F. Torsional Potentials and Full-Dimensional Simulation of Electronic Absorption and Fluorescence Spectra of *para*-Phenylene Oligomers Using the Semiempirical Self-Consistent Charge Density-Functional Tight Binding Approach. *J. Chem. Phys.* **2008**, *129*, 164905.
(38) Runge, E.; Gross, E. K. U. Density-Functional Theory for Time-Dependent Systems. *Phys. Rev. Lett.* **1984**, *52*, 997−1000.
(39) Gross, E. K. U.; Kohn, W. Local Density-Functional Theory of Frequency-Dependent Linear Response. *Phys. Rev. Lett.* **1985**, *55*, 2850−2852.
(40) Petersilka, M.; Gossmann, U. J.; Gross, E. K. U. Excitation Energies from Time-Dependent Density-Functional Theory. *Phys. Rev. Lett.* **1996**, *76*, 1212−1215.
(41) Dreuw, A.; Head-Gordon, M. Single-Reference ab Initio Methods for the Calculation of Excited States of Large Molecules. *Chem. Rev.* **2005**, *105*, 4009−4037.
(42) Casida, M. E. Time-Dependent Density-Functional Theory for Molecules and Molecular Solids. *J. Mol. Struct. (THEOCHEM)* **2009**, *914*, 3−18.
(43) Casida, M. E. Time-Dependent Density Functional Response Theory for Molecules. In *Recent Advances in Density Functional Methods*; Chong, D. P., Ed.; World Scientific: Singapore, 1995; Part I, Chapter 5, pp 155−192.
(44) Becke, A. D. Density-Functional Exchange-Energy Approximation with Correct Asymptotic Behavior. *Phys. Rev. A* **1988**, *38*, 3098−3100.
(45) Perdew, J. P. Density-Functional Approximation for the Correlation Energy of the Inhomogeneous Electron Gas. *Phys. Rev. B* **1986**, *33*, 8822−8824.
(46) Lee, C. T.; Yang, W. T.; Parr, R. G. Development of the Colle−Salvetti Correlation-Energy Formula into a Functional of the Electron Density. *Phys. Rev. B* **1988**, *37*, 785−789.
(47) Becke, A. D. Density-Functional Thermochemistry. 3. The Role of Exact Exchange. *J. Chem. Phys.* **1993**, *98*, 5648−5652.
(48) Perdew, J. P.; Burke, K.; Ernzerhof, M. Generalized Gradient Approximation Made Simple. *Phys. Rev. Lett.* **1996**, *77*, 3865−3868.
(49) Ernzerhof, M.; Scuseria, G. E. Assessment of the Perdew−Burke−Ernzerhof Exchange-Correlation Functional. *J. Chem. Phys.* **1999**, *110*, 5029−5036.
(50) Adamo, C.; Barone, V. Toward Reliable Density Functional Methods without Adjustable Parameters: The PBE0 Model. *J. Chem. Phys.* **1999**, *110*, 6158−6170.
(51) Becke, A. D. A New Mixing of Hartree−Fock and Local Density-Functional Theories. *J. Chem. Phys.* **1993**, *98*, 1372−1377.
(52) Yanai, T.; Tew, D. P.; Handy, N. C. A New Hybrid Exchange−Correlation Functional Using the Coulomb-Attenuating Method (CAM-B3LYP). *Chem. Phys. Lett.* **2004**, *393*, 51−57.
(53) Vydrov, O. A.; Scuseria, G. E. Assessment of a Long-Range Corrected Hybrid Functional. *J. Chem. Phys.* **2006**, *125*, 234109.
(54) Vydrov, O. A.; Heyd, J.; Krukau, A. V.; Scuseria, G. E. Importance of Short-Range versus Long-Range Hartree−Fock Exchange for the Performance of Hybrid Density Functionals. *J. Chem. Phys.* **2006**, *125*, 074106.
(55) Chai, J. D.; Head-Gordon, M. Long-Range Corrected Hybrid Density Functionals with Damped Atom−Atom Dispersion Corrections. *Phys. Chem. Chem. Phys.* **2008**, *10*, 6615−6620.
(56) Zhao, Y.; Truhlar, D. G. The M06 Suite of Density Functionals for Main Group Thermochemistry, Thermochemical Kinetics, Noncovalent Interactions, Excited States, and Transition Elements: Two New Functionals and Systematic Testing of Four M06-Class Functionals and 12 Other Functionals. *Theor. Chem. Acc.* **2008**, *120*, 215−241.
(57) Peverati, R.; Truhlar, D. G. Improving the Accuracy of Hybrid Meta-GGA Density Functionals by Range Separation. *J. Phys. Chem. Lett.* **2011**, *2*, 2810−2817.
(58) Rohrdanz, M. A.; Martins, K. M.; Herbert, J. M. A Long-Range-Corrected Density Functional That Performs Well for Both Ground-State Properties and Time-Dependent Density Functional Theory Excitation Energies, Including Charge-Transfer Excited States. *J. Chem. Phys.* **2009**, *130*, 054112.
(59) Gonzalez, L.; Escudero, D.; Serrano-Andres, L. Progress and Challenges in the Calculation of Electronic Excited States. *ChemPhysChem* **2012**, *13*, 28−51.
(60) Hattig, C.; Weigend, F. CC2 Excitation Energy Calculations on Large Molecules Using the Resolution of the Identity Approximation. *J. Chem. Phys.* **2000**, *113*, 5154−5161.
(61) Schirmer, J. Beyond the Random-Phase Approximation: A New Approximation Scheme for the Polarization Propagator. *Phys. Rev. A* **1982**, *26*, 2395−2416.
(62) Trofimov, A. B.; Schirmer, J. An Efficient Polarization Propagator Approach to Valence Electron-Excitation Spectra. *J. Phys. B: At. Mol. Opt. Phys.* **1995**, *28*, 2299−2324.
(63) Grimme, S. Improved Second-Order Møller-Plesset Perturbation Theory by Separate Scaling of Parallel- and Antiparallel-Spin Pair Correlation Energies. *J. Chem. Phys.* **2003**, *118*, 9095−9102.
(64) Hellweg, A.; Grun, S. A.; Hattig, C. Benchmarking the Performance of Spin-Component Scaled CC2 in Ground and Electronically Excited States. *Phys. Chem. Chem. Phys.* **2008**, *10*, 4119−4127.
(65) Weigend, F. Accurate Coulomb-Fitting Basis Sets for H to Rn. *Phys. Chem. Chem. Phys.* **2006**, *8*, 1057−1065.
(66) Weigend, F.; Ahlrichs, R. Balanced Basis Sets of Split Valence, Triple Zeta Valence and Quadruple Zeta Valence Quality for H to Rn: Design and Assessment of Accuracy. *Phys. Chem. Chem. Phys.* **2005**, *7*, 3297−3305.
(67) Ahlrichs, R.; Bar, M.; Haser, M.; Horn, H.; Kolmel, C. Electronic Structure Calculations on Workstation Computers: The Program System Turbomole. *Chem. Phys. Lett.* **1989**, *162*, 165−169.
(68) Zhao, Y.; Truhlar, D. G. Density Functionals with Broad Applicability in Chemistry. *Acc. Chem. Res.* **2008**, *41*, 157−167.
(69) Frisch, M. J.; Trucks, G. W.; Schlegel, H. B.; Scuseria, G. E.; Robb, M. A.; Cheeseman, J. R.; Scalmani, G.; Barone, V.; Mennucci, B.; Petersson, G. A.; Nakatsuji, H.; Caricato, M.; Li, X.; Hratchian, H. P.; Izmaylov, A. F.; Bloino, J.; Zheng, G.; Sonnenberg, J. L.; Hada, M.; Ehara, M.; Toyota, K.; Fukuda, R.; Hasegawa, J.; Ishida, M.; Nakajima,

DOI: 10.1021/acs.jpca.5b00354
J. Phys. Chem. A 2015, 119, 6937−6948

T.; Honda, Y.; Kitao, O.; Nakai, H.; Vreven, T.; Montgomery, J. A., Jr.; Peralta, J. E.; Ogliaro, F.; Bearpark, M.; Heyd, J. J.; Brothers, E.; Kudin, K. N.; Staroverov, V. N.; Keith, T.; Kobayashi, R.; Normand, J.; Raghavachari, K.; Rendell, A.; Burant, J. C.; Iyengar, S. S.; Tomasi, J.; Cossi, M.; Rega, N.; Millam, J. M.; Klene, M.; Knox, J. E.; Cross, J. B.; Bakken, V.; Adamo, C.; Jaramillo, J.; Gomperts, R.; Stratmann, R. E.; Yazyev, O.; Austin, A. J.; Cammi, R.; Pomelli, C.; Ochterski, J. W.; Martin, R. L.; Morokuma, K.; Zakrzewski, V. G.; Voth, G. A.; Salvador, P.; Dannenberg, J. J.; Dapprich, S.; Daniels, A. D.; Farkas, Ö.; Foresman, J. B.; Ortiz, J. V.; Cioslowski, J.; Fox, D. J. *Gaussian 09*, revision B.01. Gaussian, Inc.: Wallingford, CT, 2009.

(70) Verlet, L. Computer Experiments on Classical Fluids. I. Thermodynamical Properties of Lennard-Jones Molecules. *Phys. Rev.* **1967**, *159*, 98−103.

(71) Domcke, W.; Yarkony, D. R.; Köppel, H. *Conical Intersections: Theory, Computation and Experiment*; Advanced Series in Physical Chemistry; World Scientific: Singapore, 2011; Vol. *17*.

(72) Tavernelli, I.; Tapavicza, E.; Rothlisberger, U. Nonadiabatic Dynamics Using Time-Dependent Density Functional Theory: Assessing the Coupling Strengths. *J. Mol. Struct. (THEOCHEM)* **2009**, *914*, 22−29.

(73) Hammes-Schiffer, S.; Tully, J. C. Proton Transfer in Solution: Molecular Dynamics with Quantum Transitions. *J. Chem. Phys.* **1994**, *101*, 4657−4667.

(74) Mitrić, R.; Werner, U.; Wohlgemuth, M.; Seifert, G.; Bonacic-Koutecky, V. Nonadiabatic Dynamics within Time-Dependent Density Functional Tight Binding Method. *J. Phys. Chem. A* **2009**, *113*, 12700−12705.

(75) Tapavicza, E.; Tavernelli, I.; Rothlisberger, U.; Filippi, C.; Casida, M. E. Mixed Time-Dependent Density-Functional Theory/Classical Trajectory Surface-Hopping Study of Oxirane Photochemistry. *J. Chem. Phys.* **2008**, *129*, 124108.

(76) Mitrić, R.; Werner, U.; Bonacic-Koutecky, V. Nonadiabatic Dynamics and Simulation of Time Resolved Photoelectron Spectra within Time-Dependent Density Functional Theory: Ultrafast Photoswitching in Benzylideneaniline. *J. Chem. Phys.* **2008**, *129*, 164118.

(77) Tapavicza, E.; Tavernelli, I.; Rothlisberger, U. Trajectory Surface Hopping within Linear Response Time-Dependent Density-Functional Theory. *Phys. Rev. Lett.* **2007**, *98*, 023001.

(78) Wohlgemuth, M.; Bonacic-Koutecky, V.; Mitrić, R. Time-Dependent Density Functional Theory Excited State Nonadiabatic Dynamics Combined with Quantum Mechanical/Molecular Mechanical Approach: Photodynamics of Indole in Water. *J. Chem. Phys.* **2011**, *135*, 054105.

(79) Casida, M. E.; Huix-Rotllant, M. Progress in Time-Dependent Density-Functional Theory. *Annu. Rev. Phys. Chem.* **2012**, *63*, 287−323.

(80) Barbatti, M.; Pittner, J.; Pederzoli, M.; Werner, U.; Mitric, R.; Bonacic-Koutecky, V.; Lischka, H. Nonadiabatic Dynamics of Pyrrole: Dependence of Deactivation Mechanisms on the Excitation Energy. *Chem. Phys.* **2010**, *375*, 26−34.

(81) Pittner, J.; Lischka, H.; Barbatti, M. Optimization of Mixed Quantum-Classical Dynamics: Time-Derivative Coupling Terms and Selected Couplings. *Chem. Phys.* **2009**, *356*, 147−152.

(82) Subotnik, J. E. Fewest-Switches Surface Hopping and Decoherence in Multiple Dimensions. *J. Phys. Chem. A* **2011**, *115*, 12083−12096.

(83) Fang, J. Y.; Hammes-Schiffer, S. Improvement of the Internal Consistency in Trajectory Surface Hopping. *J. Phys. Chem. A* **1999**, *103*, 9399−9407.

(84) Zhu, C. Y.; Nangia, S.; Jasper, A. W.; Truhlar, D. G. Coherent Switching with Decay of Mixing: An Improved Treatment of Electronic Coherence for Non-Born-Oppenheimer Trajectories. *J. Chem. Phys.* **2004**, *121*, 7658−7670.

(85) Subotnik, J. E.; Shenvi, N. Decoherence and Surface Hopping: When Can Averaging over Initial Conditions Help Capture the Effects of Wave Packet Separation? *J. Chem. Phys.* **2011**, *134*, 244114.

(86) Subotnik, J. E.; Ouyang, W. J.; Landry, B. R. Can We Derive Tully's Surface-Hopping Algorithm from the Semiclassical Quantum Liouville Equation? Almost, but Only with Decoherence. *J. Chem. Phys.* **2013**, *139*, 214107.

(87) Shenvi, N.; Subotnik, J. E.; Yang, W. T. Simultaneous-Trajectory Surface Hopping: A Parameter-Free Algorithm for Implementing Decoherence in Nonadiabatic Dynamics. *J. Chem. Phys.* **2011**, *134*, 144102.

(88) Landry, B. R.; Subotnik, J. E. Communication: Standard Surface Hopping Predicts Incorrect Scaling for Marcus' Golden-Rule Rate: The Decoherence Problem Cannot Be Ignored. *J. Chem. Phys.* **2011**, *135*, 191101.

(89) Granucci, G.; Persico, M. Critical Appraisal of the Fewest Switches Algorithm for Surface Hopping. *J. Chem. Phys.* **2007**, *126*, 134114.

(90) Levine, B. G.; Ko, C.; Quenneville, J.; Martínez, T. J. Conical Intersections and Double Excitations in Time-Dependent Density Functional Theory. *Mol. Phys.* **2006**, *104*, 1039−1051.

(91) Thiel, W. *MNDO*, version 6.1; Max-Planck-Institut für Kohlenforschung, Mülheim an der Ruhr, Germany, 2007.

(92) Voityuk, A. A. Fragment Transition Density Method to Calculate Electronic Coupling for Excitation Energy Transfer. *J. Chem. Phys.* **2014**, *140*, 244117.

(93) Plasser, F.; Aquino, A. J. A.; Hase, W. L.; Lischka, H. Uv Absorption Spectrum of Alternating DNA Duplexes. Analysis of Excitonic and Charge Transfer Interactions. *J. Phys. Chem. A* **2012**, *116*, 11151−11160.

(94) Plasser, F.; Lischka, H. Analysis of Excitonic and Charge Transfer Interactions from Quantum Chemical Calculations. *J. Chem. Theory Comput.* **2012**, *8*, 2777−2789.

(95) Settels, V.; Liu, W. L.; Pflaum, J.; Fink, R. F.; Engels, B. Comparison of the Electronic Structure of Different Perylene-Based Dye-Aggregates. *J. Comput. Chem.* **2012**, *33*, 1544−1553.

(96) Huang, J.; Du, L. K.; Hu, D. P.; Lan, Z. G. Theoretical Analysis of Excited States and Energy Transfer Mechanism in Conjugated Dendrimers. *J. Comput. Chem.* **2015**, *36*, 151−163.

(97) Liu, K. L.; Lee, S. J.; Chen, I. C.; Hsu, C. P.; Yeh, M. Y.; Luh, T. Y. Excited-State Dynamics of [(1,1′-Biphenyl)-4,4-diyldi-2,1-ethenediyl]bis(dimethylsilane). *J. Phys. Chem. A* **2009**, *113*, 1218−1224.

(98) Sluch, M. I.; Godt, A.; Bunz, U. H. F.; Berg, M. A. Excited-State Dynamics of Oligo(*p*-phenyleneethynylene): Quadratic Coupling and Torsional Motions. *J. Am. Chem. Soc.* **2001**, *123*, 6447−6448.

(99) Cailleau, H.; Baudour, J. L.; Meinnel, J.; Dworkin, A.; Moussa, F.; Zeyen, C. M. E. Double-Well Potentials and Structural Phase Transitions in Polyphenyls. *Faraday Discuss.* **1980**, *69*, 7−18.

(100) Karabunarliev, S.; Baumgarten, M.; Bittner, E. R.; Mullen, K. Rigorous Franck−Condon Absorption and Emission Spectra of Conjugated Oligomers from Quantum Chemistry. *J. Chem. Phys.* **2000**, *113*, 11372−11381.

(101) Wenzel, J.; Dreuw, A.; Burghardt, I. Charge and Energy Transfer in a Bithiophene Perylenediimide Based Donor−Acceptor−Donor System for Use in Organic Photovoltaics. *Phys. Chem. Chem. Phys.* **2013**, *15*, 11704−11716.

DOI: 10.1021/acs.jpca.5b00354
J. Phys. Chem. A 2015, 119, 6937−6948